Estimation of surface-layer scaling parameters in the unstable boundary layer: implications for orographic flow speed-up

Article

Accepted Version

It is advisable to refer to the publisher's version if you intend to cite from the work. See Guidance on citing.

1   # Estimation of surface-layer scaling parameters in the unstable

2   # boundary-layer: implications for orographic flow speed-up

3

4   **José Luís Argaín • Miguel A. C. Teixeira • Pedro M. A. Miranda**

5

6

8   **Abstract** A method is proposed for estimating the surface-layer depth (z_s) and the
9   friction velocity (u_*) as a function of stability (here quantified by the Obukhov length, L)
10   over the complete range of unstable flow regimes. This method extends the one
11   developed previously by the authors for stable conditions in Argaín et al. (Boundary-
12   Layer Meteorol, 2009, Vol.130, 15-28), but uses a qualitatively different approach. The
13   method is specifically used to calculate the fractional speed-up (ΔS) in flow over a ridge,
14   although it is suitable for more general boundary-layer applications. The behaviour of
15   $z_s(L)$ and $u_*(L)$ as a function of L is indirectly assessed via calculation of $\Delta S(L)$ using
16   the linear model of Hunt et al. (Q J R Meteorol Soc, 1988, Vol.29, 16-26) and its
17   comparison with the field measurements reported in Coppin et al. (Boundary-Layer
18   Meteorol, 1994, Vol.69, 173-199) and with numerical simulations carried out using a
19   nonlinear numerical model, FLEX. The behaviour of ΔS estimated from the linear model
20   is clearly improved when u_* is calculated using the method proposed here, confirming
21   the importance of accounting for the dependences of $z_s(L)$ and $u_*(L)$ on L to better
22   represent processes in the unstable boundary-layer.

23

José Luis Argaín
Departamento de Física, FCT, Universidade do Algarve, Faro 8005-139, Portugal.
jargain@ualg.pt

Miguel Ângelo Cortez Teixeira
Department of Meteorology, University of Reading, Earley Gate, PO Box 243, Reading RG6 6BB, UK
m.a.teixeira@reading.ac.uk

Pedro Manuel Alberto de Miranda
Instituto Dom Luiz, Faculdade de Ciências, Universidade de Lisboa, Lisbon 1749-016, Portugal
pmmiranda@fc.ul.pt

26

1 Introduction

28   Fractional speed-up (ΔS) of flow over hills or mountains is defined as the ratio of the

29   speed perturbation at a given height to the upstream, unperturbed flow speed at the same

30   height. This quantity is highly relevant both from meteorological and wind engineering

31   perspectives, since it characterizes the modulation of the wind speed by orography. Hunt

32   et al. (1988) (hereafter HLR) developed one of the first theoretical linear atmospheric

33   boundary layer (ABL) models of flow over hills, which is one of the simplest and

34   computationally cheapest tools available for estimating ΔS.

35   However, stratification affects ΔS and must be carefully accounted for in the evaluation

36   of the scaling parameters that characterize the ABL. Among these, a key parameter is the

37   friction velocity (u_*), and another one is the surface-layer depth (z_s), usually estimated as

38   5% to 10% of the ABL depth.

39   Weng (1997) (hereafter W97), after implementing a continuous wind profile in the HLR

40   model, found that his predictions of ΔS disagreed significantly with the observations of

41   Coppin et al. (1994) (hereafter C94). Argaín et al. (2009) (hereafter A09) showed that

42   these discrepancies were due to the fact that the calculations in W97 were carried out

43   assuming that u_* is constant, regardless of the different observed stability regimes. They

44   proposed a method for estimating u_* in stably-stratified flows, which has led to an

45   improved prediction of ΔS over 2D hills. C94 also compared their observations with

46   predictions from the HLR model, and found considerable disagreement, both in stable

47   and unstable conditions. Here we show that, as in stably-stratified flows, a decisive

48   reason for such disagreements in unstable flow is the assumption of constant u_*.

49   In the present study, a new method is developed for estimating z_s and u_* as a function of

50   stability (here quantified by the Obukhov length, L) over the complete unstable

51   stratification range, i.e. from the free-convection to the neutral stability limits. Procedures

52   are developed for estimating z_s in a neutral ABL, and for estimating this and several

53   other scaling parameters, such as u_*, L and Deardorff's convective velocity scale, w_*, in

54   the free-convection regime, which are preliminary steps for defining $z_s(L)$ and $u_*(L)$ for

55   all stabilities. Given that the physical processes taking place in the CBL and in an
56   unstable surface layer are substantially different from those in a stable boundary ABL,
57   the method used to represent them also differs substantially, requiring the use of
58   additional theory.

59   The main motivation for developing this new method for estimating $z_s(L)$ and $u_*(L)$ is
60   the calculation of $\Delta S(L)$ for unstable flow over hills, although it must be noted that the
61   method can also be used for more general boundary layer applications. The calculation of
62   $\Delta S(L)$ requires knowing $u_*(L)$ which, in the method proposed here, also requires
63   estimating $z_s(L)$. The behaviour of $z_s(L)$ and $u_*(L)$ is thus indirectly assessed through
64   the calculation of $\Delta S(L)$ using the HLR model. These predictions are compared with field
65   measurements, reported in C94, and numerical simulations, carried out using a 2D
66   microscale-mesoscale non-hydrostatic model, FLEX. These comparisons allow us to
67   show how $z_s(L)$ and $u_*(L)$ are sometimes not estimated in a physically consistent way, a
68   limitation that the present method aims to overcome.

69   Section 2 presents the method that accounts for unstable stratification in the ABL and its
70   calibration. Section 3 describes the main results, namely comparisons between theory,
71   numerical simulations and measurements, using the new unstable ABL formulation.
72   Finally, Sect. 4 summarizes the main conclusions of this study.

73

74   **2 Methodology**

75   2.1 Unstable ABL model

76   Several studies show that the ABL, under moderately to strongly unstable stratification
77   (usually known as CBL), can be represented by a simplified three-layer bulk model (e.g.,
78   Garratt 1992). This comprises a thin statically unstable surface layer of depth z_s, a well-
79   mixed layer, of height z_i and depth $\Delta z_i = z_i - z_s$, and a transition layer of thickness
80   Δz_{ci}, coinciding with a temperature inversion capping the mixed layer, which inhibits
81   vertical mixing. In the mixed layer, quantities such as the mean potential temperature (θ)
82   and wind velocity (U,V) are well-mixed, and therefore constant with height, i.e. $\theta(z) =$
83   $const.$, $U(z) = const.$ and $V(z) = 0$. For our purposes, the strict fulfilment of these
84   profile shapes in the mixed layer is not critical, since we are essentially interested in the
85   surface layer, for which typically $z_s \approx 0.05z_i$ to $0.1z_i$ (Stull 1988). In the surface layer we

86　　assume that the turbulent shear stresses have much more important effects on the mean

87　　flow than the Coriolis force. Hence, the Coriolis parameter (f) is set to zero, except

88　　where otherwise explicitly stated. Since the surface layer has characteristics which make

89　　it markedly different from the mixed layer, z_s can be defined as an important length scale

90　　of the ABL, essential for describing the impact of the orography on the wind profile. This

91　　follows McNaughton (2004), who established z_s as a new basis parameter for similarity

92　　models of the surface layer. In the method proposed here, z_s is essential for estimating

93　　the key velocity scale, u_*, and hence for calculating $\Delta S(L)$.

94

95　　2.2 Surface-layer model

96　　According to Monin-Obukhov similarity theory (MOST), in the surface layer the non-

97　　dimensional vertical gradients of $U(z)$ and $\theta(z)$ are universal functions of the parameter

98　　z/L, taking the forms

99
$$\Phi_m\left(\frac{z}{L}\right) = \frac{\kappa z}{u_*}\frac{\partial U}{\partial z},\tag{1}$$

100　　and

101
$$\Phi_h\left(\frac{z}{L}\right) = \frac{\kappa z}{Pr_t\,\theta_*}\frac{\partial \theta}{\partial z},\tag{2}$$

102　　where z is the height above the effective ground level, κ is the von Kármán constant,

103　　Pr_t is the turbulent Prandtl number and θ_* represents the surface-layer scaling

104　　temperature. u_* and θ_*, are defined using the vertical eddy kinematic fluxes of

105　　momentum and heat at the surface, i.e. $u_*^2 = \left(\overline{w'u'}\right)_0$ and $\theta_* = -\left(\overline{w'\theta'}\right)_0/u_*$. The length

106　　L is given by

107
$$L = -\frac{\theta_0 u_*^3/\kappa}{g\left(\overline{w'\theta'}\right)_0} = \frac{\theta_0 u_*^2}{g\kappa\theta_*},\tag{3}$$

108　　where θ_0 is the potential temperature at the surface and g is the gravitational

109　　acceleration. Wilson (2001) (hereafter W01), after analyzing several forms of the

110　　functions Φ_m and Φ_h, proposed the following general form for the unstable regime (z/L

111　　< 0),

4

$$\Phi = \left(1 + \gamma\left|\frac{z}{L}\right|^{\alpha_1}\right)^{-\alpha_2}, \tag{4}$$

112

113   which is valid for both Φ_m and Φ_h. He noted that in order to obtain the correct physical

114   behaviour for the gradients $\partial U/\partial z$ and $\partial\theta/\partial z$ in the free-convection limit ($z/L \to -\infty$), it

115   is required that $\alpha_1\alpha_2 = 1/3$. For this combination of values (4) behaves in this limit

116   similarly to 'classical' free-convection expressions, with $\partial U/\partial z$ and $\partial\theta/\partial z$ varying

117   proportionally to $z^{-4/3}$. He further noted that, for this choice of parameters, (1) - (2) may

118   be integrated straightforwardly. Following W01 we will use $\kappa = 0.4$, $Pr_t = 0.95$, $\gamma_h =$

119   7.86, $\alpha_{1m} = \alpha_{1h} = 2/3$, $\alpha_{2m} = \alpha_{2h} = 1/2$ and $\gamma_m = 3.59$.

120   Subscripted indices s, n and fc hereafter denote values of flow parameters in the surface

121   layer, in the neutral regime ($|L| \to \infty$), and in the free-convection regime ($|L| \to 0$),

122   respectively.

123   The method developed here requires that z_{sfc}, u_{*fc}, L_{fc}, z_{sn}, u_{*n} and z_0, be known in

124   order to calculate $u_*(L)$ and $z_s(L)$. The primary input parameters are u_{*n}, z_{ifc} and the

125   aerodynamic roughness height, z_0, which must be provided initially.

126

127   2.3 Estimating parameters in the free-convection and neutral regimes

128   MOST shows good agreement with observations in regimes with sufficiently strong

129   winds (high values of u_*) or under relatively low surface heat flux, $\overline{(w'\theta)}_0$, where $|L| >$

130   10^2 m. This theory is based on the assumption that, in the surface layer, z and L are the

131   only relevant turbulence length scales. While this assumption is valid for relatively small

132   values of $|z/L|$ (say $|z/L| < 1$), for larger values, in particular in the free-convection

133   regime, MOST becomes incomplete. In the perfectly windless regime, purely dominated

134   by thermal effects, both the mean wind speed and u_* approach zero, and MOST produces

135   singularities and underestimates the surface fluxes. However, perfectly windless

136   conditions occur very rarely, and the theory can still be applied, if conjugated with CBL

137   theory, for low but non-zero winds, as will be shown below.

138   For the highly convective ABL, Deardorff (1970) suggested the following convective

139   velocity scale

140
$$w_* = \left[\frac{g}{\theta_0} \left(\overline{w'\theta'} \right)_0 z_{ifc} \right]^{1/3}.$$
(5)

141 The combination of MOST and Deardorff similarity theory, adopted here, provides a

142 model that is consistent throughout the whole CBL (Kaimal et al. 1976) (hereafter K76),

143 and for stabilities ranging from the neutral regime to the free-convection regime. This

144 latter regime does not strictly correspond to $L = 0$, but rather to a minimum, suitably

145 small value of $L = L_{fc}$, to be determined. In the free-convection regime we need to

146 estimate z_{sfc}, u_{*fc} and L_{fc}. Given that u_{*fc} is defined in relation to w_* (as shown

147 below), this latter quantity, defined by (5), must also be related to the known input

148 parameters. This requires a total of four equations (see below).

149 Many observations have confirmed that the transition from the shear-driven turbulent

150 regime of the surface layer to the buoyancy driven regime of the mixed layer usually

151 occurs at a height of order $|L|$. Hence, in a highly-convective ABL (Garratt 1992),

152
$$z_{sfc} = c_{fc} \left| L_{fc} \right|,$$
(6)

153 where $c_{fc} = 2$. Equation 6 will be adopted hereafter in the free-convection regime.

154 Based on observations, Schumann (1988) (hereafter S88) assumed that $z_s/z_i = 0.1$. As

155 will be seen later, this assumption is too restrictive over the whole stability interval,

156 since, z_i is expected to increase and z_s to decrease as the stratification becomes more

157 unstable. A more general definition of z_s is thus required. This is developed in Sect. 2.4.

158 Businger (1973) proposed the idea that u_* does not vanish at low wind speeds,

159 introducing the concept of a 'minimum friction velocity', valid in the free-convection

160 regime ($u_{*min} = u_{*fc}$). Combining (3) and (5) in this regime, we obtain

161
$$\frac{\kappa \left| L_{fc} \right|}{z_{ifc}} = \left(\frac{u_{*fc}}{w_*} \right)^3.$$
(7)

162 Using (6), it can be easily shown from (7) that z_{sfc}/z_{ifc} decreases as u_{*fc}/w_* decreases,

163 which is physically plausible.

164 Various authors, such as S88 and Sykes et al. (1993) (hereafter S93), have advocated the

165 view that u_{*fc}/w_* is a function of z_{sfc}/z_0 or z_{ifc}/z_0 as well. Following the less general

166 relations derived by S88 and S93, valid only for limited intervals of z_0, Zilitinkevich et

167 al. (2006) (hereafter Z06) suggested a more complete formulation for the relationship

168 between u_{*fc}/w_* and z_{ifc}/z_0, which takes into account the combined effects of

169 buoyancy and shear forces,

170
$$\frac{u_{*fc}}{w_*} = c_1 \left[\ln \frac{z_{ifc}/z_0}{\left(\ln z_{ifc}/z_0 - c_0 \right)^3} + c_2 \right]^{-1} \qquad \text{for } z_{ifc}/z_0 \geq \sigma, \qquad (8)$$

171
$$\frac{u_{*fc}}{w_*} = c_3 \left[\frac{z_0}{z_{ifc}} + c_4 \left(\frac{z_0}{z_{ifc}} \right)^{8/7} \right]^{1/6} \qquad \text{for } z_{ifc}/z_0 < \sigma, \qquad (9)$$

172 where $\sigma = 3.45 \times 10^5$, $u_{*fc}/w_*(\sigma) = 0.065$, $c_0 = 6.00$, $c_1 = 0.29$, $c_2 = -2.56$, $c_3 = 0.54$

173 and $c_4 = 0.3$. Equations 8 and 9 agree very well with both LES and field data in the free-

174 convection regime (Z06), and incorporate the best characteristics of the S88 and S93

175 models.

176 The height z_i characterizes the PBL in a fairly integrated manner, being closely related to

177 fundamental quantities such as $\left(\overline{w'\theta'} \right)_0$. For this reason, as a first approach, we suggest

178 estimating the surface-layer scaling parameters in the free-convection regime based on a

179 known value of z_{ifc}. This allows obtaining u_{*fc}/w_* directly from (8) - (9), since z_0 is

180 also assumed to be known.

181 Our final constraint is based on Venkatram (1978) who, by using a simple mixed-layer

182 model for the CBL, derived the following relationship between w_* and z_{ifc},

183
$$w_* = c_5 z_{ifc}, \qquad (10)$$

184 where $c_5 = 1.12 \times 10^{-3}$ s^{-1}. Equation 10 compares extremely well with observations (see

185 Appendix 2). Using the available value of z_{ifc}, (10) allows us to determine w_* directly.

186 Equations 6 - 10 may thus be used to obtain the surface-layer parameters in the free-

187 convection regime, as follows. Given z_{ifc} and z_0, (8) or (9) is used to obtain u_{*fc}/w_*

188 and (10) is used to obtain w_*, which yields u_{*fc}. Given z_{ifc}, w_* and u_{*fc}, determined in

189 the preceding step, (7) is used to obtain L_{fc}. Finally, L_{fc} is inserted into (6) to obtain z_{sfc}.

190 This yields u_{*fc}, L_{fc} and z_{sfc}, as required. Several different procedures analogous to the

191 one just described would be possible, depending on what input parameters are known

192 initially.

193   According to MOST, in the neutral regime

$$U_n(z) = \frac{u_{*n}}{\kappa} \ln\left(\frac{z}{z_0}\right). \tag{11}$$

195   Since, from (6), z_s is expected to depend on L, in the neutral regime at least (where no
196   stability effects exist), it seems reasonable to assume z_s to be a fixed fraction of z_i (Stull
197   1988),

$$z_{sn} = c_{SL} \, z_{in}, \tag{12}$$

199   where that fraction is conventionally defined as 5% to 10% of z_i (Stull 1988). In our
200   model, we assume $c_{SL} = 0.05$ (following Stull 2011). Here, and unlike what previous
201   authors have done, (12) is adopted only for the strictly neutral regime. As will be seen
202   later (Sect. 3.2), (12) holds approximately for a weakly unstable ABL, but not for a
203   strongly unstable ABL. In order to obtain z_{sn} from (12), it is still necessary to estimate
204   z_{in}. This can be done using the expression of Rossby and Montgomery (1935),

$$z_{in} = \frac{c_{zin} u_{*n}}{|f|}, \tag{13}$$

206   where $c_{zin} = 0.2$ (Garratt 1992).

207

208   2.4 Estimating z_s and u_* for arbitrary $L < 0$

209   The preceding section described the methodologies for estimating all the parameters
210   required for defining u_* and z_s in the free-convection and neutral regimes. Next we
211   explain the approach used to estimate these two parameters for arbitrary $L < 0$.

212   Since $|L|$ is the height at which the buoyant production of turbulence kinetic energy (E)
213   begins to dominate over shear production, the greater $\left(\overline{w'\theta'}\right)_0$ is (i.e. the smaller $|L|$ is),
214   the bigger Δz_i and the smaller z_s become, because convectively-driven turbulence
215   increasingly dominates over shear-driven turbulence. So, there is a clear relationship
216   between z_s and $|L|$ (expressed by (6) in the strongly unstable regime). However, for
217   intermediate unstable regimes the dependence $z_s(L)$ is not known.

218   Based on the ABL model described in Sect. 2.1, we define z_s as the height where the
219   vertical derivative of $\theta(z)$ reaches a small prescribed fraction of its surface value. Using

220 this property, in the present model $z_s(L)$ is determined by (see details in Appendix 1)

221 evaluating the root of,

$$\frac{z_s}{z_{0\theta}} = \frac{1}{\alpha_{\Psi 2}} \left(\frac{z_{0\theta}}{z_s} \right)^{-\alpha_{\Psi 1}} \left[\frac{1 + \gamma_h \left(z_s / |L| \right)^{\alpha_1}}{1 + \gamma_h \left(z_{0\theta} / |L| \right)^{\alpha_1}} \right]^{-\alpha_2}, \qquad (14)$$

223 for any value of L, assuming that $z_{0\theta}$, α_1, α_2, γ_h, $\alpha_{\Psi 1}$ and $\alpha_{\Psi 2}$ are provided. As (14)

224 includes the influence on $z_s(L)$ of parameters in both extremes of the stability interval

225 (see Appendix 1), it is expected to provide a good approximation over the whole stability

226 range. As the roughness length for heat, $z_{0\theta}$, is not provided by C94, we use here z_0

227 instead. Calculations not presented here show that the $z_s(L)$ dependences obtained using

228 $z_{0\theta}/z_s$ or z_0/z_s are quite similar (the relation between $z_{0\theta}$ and z_0 assumed for this

229 comparison follows Zilitinkevich 1995). Although $z_{0\theta}$ and z_0 differ, the proposed method

230 for estimating z_s is not very sensitive to the exact value of z_0 as long as this is small.

231 $u_*(L)$, on the other hand, is calculated from

$$u_*(z_s, L) = \kappa z_s \left[1 + \gamma_m \left(\frac{z_s}{|L|} \right)^{\alpha_1} \right]^{\alpha_2} \left(\frac{\partial U}{\partial z} \right)_{z_s}, \qquad (15)$$

233 where, in accordance with the slab model adopted initially (see Sect. 2.1), it is expected

234 that $\partial U / \partial z$ becomes small as $z \to z_s$. Here we assume that in (15) the shear $(\partial U / \partial z)_{z_s}$

235 is constant, and, for convenience, equal to its neutral value. For $|L| \to \infty$ and at $z = z_s$,

236 (1) reduces to $(\partial U / \partial z)_{z_{sn}} = u_{*n} / (\kappa z_{sn})$, in accordance with (11), where z_{sn} may be

237 obtained from (12). The validity of the assumption $(\partial U / \partial z)_{z_s} = const.$ is tested in

238 Appendix 2.

239 All quantities on the right-hand side of (15) are now known, and hence $u_*(z_s, L)$ may be

240 determined in general. Finally, the $U(z)$ profile for the general unstably stratified case,

241 which will be used in the HLR model for calculating $\Delta S(L)$,

$$U(z) = \frac{u_*}{\kappa} \left\{ \ln \left(\frac{z}{z_0} \right) - 3 \ln \left[\frac{1 + \sqrt{1 + \gamma_m \left(z / |L| \right)^{2/3}}}{1 + \sqrt{1 + \gamma_m \left(z_0 / |L| \right)^{2/3}}} \right] \right\}, \qquad (16)$$

243 is obtained by integration of (1), using the velocity gradient expressed by (4) (see W01).

9

244   In the above treatment, it was assumed that the synoptic situation does not vary too

245   rapidly compared with the time scales of flow over the ridge. Hence, according to MOST,

246   the effect of L in the surface layer is dominant. As this quasi-steadiness is supported by

247   the C94 campaign, the C94 observations can safely be used for testing the method

248   proposed here. For more unsteady flows, it is likely necessary to use a time-dependent

249   model for the whole ABL, such as that described by Weng and Taylor (2003), for

250   providing upstream profiles $U(z)$ and $\theta(z)$ at different values of L. However, this

251   approach would require more input parameters not available in the C94 observations, and

252   their estimation would further increase the empiricism of the proposed method.

253   Summarizing, in this section, assuming that z_0, z_{sfc}, L_{fc}, z_{sn} and u_{*n} are known, we

254   propose (14) and (15) for determining $z_s(L)$ and $u_*(L)$, respectively. $u_*(L)$ is then used

255   in the HLR model to calculate $\Delta S(L)$ for flow over orography.

256

257   **3 Results and discussion**

258   The method presented above will be assessed using the observations of C94. These

259   measurements were conducted during the Spring of 1984 and Summer of 1985, over

260   Cooper's Ridge, located to the north-west of Goulburn, in New South Wales, Australia.

261   This is a somewhat isolated north-south oriented, quasi-two-dimensional ridge of uniform

262   low z_0, located along a valley that forces the air to flow over the hill predominantly from

263   the west side. The windward slope of the ridge (west side) can be well fitted using a

264   simple bell-shaped profile $h(x) = h_0/\{1 + (x/a)^2\}$ (with $h_0 = 115$ m and $a = 400$ m).

265   The lee side of the ridge falls away to about $0.5h_0$ before rising to another broader ridge.

266

267   3.1 Estimation of parameter values from the data

268   As mentioned in Sect. 2, for determining $z_s(L)$ and $u_*(L)$, the method developed here

269   requires that z_0, z_{sfc}, u_{*fc}, L_{fc}, z_{sn} and u_{*n} be known. From the data collected by C94,

270   we have $u_{*n} = 0.35$ m s^{-1}, $z_0 = 0.05$ m and $f \approx 9 \times 10^{-5}$ s^{-1}. Using (13) we thus obtain z_{in}

271    $= 778$ m, and using this value in (12) yields $z_{sn} = 39$ m.

272   The methodology described in Sect. 2.3 for estimating the flow parameters in the free-

273   convection regime (z_{sfc}, u_{*fc}, L_{fc} and w_*) is now applied. As z_{ifc} is not supplied by

274   C94, we will use a typical value corresponding to the season and latitude of the region

where the observations were taken. Figures containing the necessary information from ERA-40 Reanalysis, provided by Von Engeln and Teixeira (2013), suggest $z_{ifc} = 1550$ m. Next, since $z_{ifc}/z_0 = 3 \times 10^4 < \sigma = 3.45 \times 10^5$, we must use (9) to calculate $u_{*fc}/w_* = 0.098$. Substituting u_{*fc}/w_* and z_{ifc} into (7), we obtain $L_{fc} = -3.6$ m, and from (6) we obtain $z_{sfc} = 7.2$ m. Next, substitution of z_{ifc} in (10) gives $w_* = 1.74$ m s^{-1}, which in turn can be used for calculating u_{*fc} from $u_{*fc}/w_* = 0.098$, yielding $u_{*fc} = 0.17$ m s^{-1}. Table 1 presents known and estimated parameters of the ABL in the free-convection regime, obtained by the present method and, for comparison, observations from runs 6A1 and 6A2 of the field experiment reported by K76, corresponding to a highly convective ABL. As can be seen, the method proposed here seems to predict realistic results.

Source	u_{*fc} (m s^{-1})	$\lvert L_{fc}\rvert$ (m)	z_{sfc} (m)	z_{ifc} (m)	z_{sfc}/z_{ifc}	w_* (m s^{-1})	u_{*fc}/w_*
Present method	0.17	3.6	7.2	1550	0.005	1.70	0.098
Run 6A1	0.24	5.7	10.4	2095	0.005	2.43	0.099
Run 6A2	0.23	6.4	12.8	2035	0.006	2.21	0.104

Table 1 Parameters of the ABL in the free-convection regime. Line 1: parameters used in the present method. Lines 2-3: similar parameters from runs 6A1 and 6A2 of the experiment described in Kaimal et al. (1976). The value of z_{sfc} for these runs was obtained from (6).

It is interesting that, contrary to what happens in the neutral regime, the ratio $z_{sfc}/z_{ifc} = 0.005$, estimated above, is significantly lower than the value assumed in (12). This value is of the same order of magnitude as those derived from the measurements of K76, taken in strongly convective conditions (see Table 1). As pointed out before, the smaller $\lvert L\rvert$ is, the more intense the turbulent mixing by large convective eddies in the mixed layer becomes, thereby reducing z_s. This corroborates, using real data, that the neutral approximation for z_{sn}/z_{in} cannot be considered realistic over the whole range of variation of L, particularly near the free-convection regime.

3.2 Behaviour of z_s as a function of L

For a better understanding of the surface-layer structure, it is useful to define a transition height, z_{tr}, at which the convective contribution to $U(z)$ is as important as that of the

302   neutral log law. Following Kader and Yaglom (1990), from the W01 formulation (4), we

303   can define

$$z_{tr} = |L| \gamma_m^{-1/\alpha_1} . \qquad (17)$$

305   It is expected that, in moderately to strongly unstable flow regimes $z_{tr} < z_s$, i.e. at the top

306   of the surface layer $U(z)$ is no longer logarithmic.

307   Figure 1 presents the variation of z_s and z_{tr}, with $|L|$, normalized by z_{sn}. The solid line

308   represents $z_s(L)$, computed using (14). In (14), the coefficients $\alpha_{\Psi 1}$ and $\alpha_{\Psi 2}$, given by

309   (23), take the values 0.415 and 0.018, respectively. $z_{tr}(L)$ (dashed line) is computed

310   using (17).

311

312
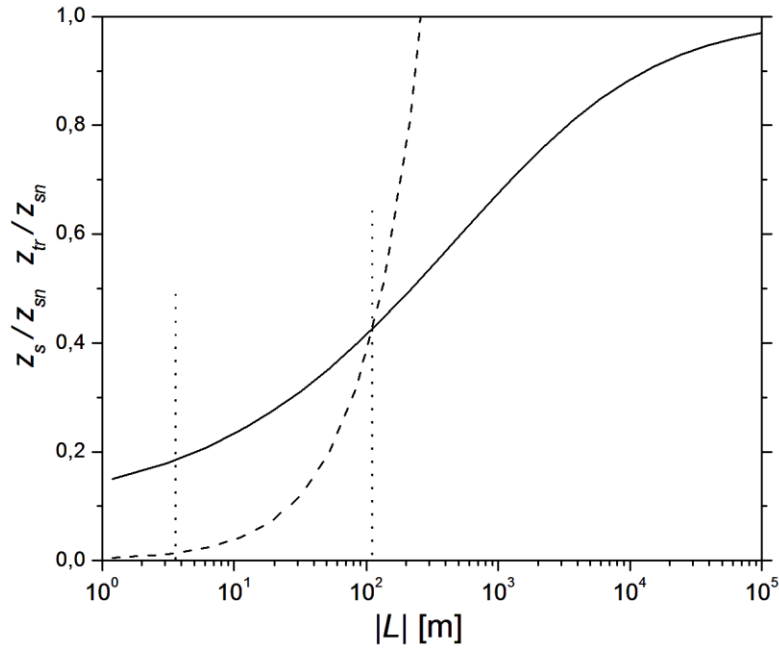
313   **Fig 1** Surface-layer height, z_s, and transition height, z_{tr}, as a function of $|L|$, normalized by the surface-

314   layer height for a neutral ABL, z_{sn}. Solid line: $z_s(L)$ obtained from (14), dashed line: $z_{tr}(L)$ obtained from

315   (17). Vertical dotted lines: $|L_{fc}| = 3.6$ m (left), and $|L_{tr}| = 120$ m (right). $z_s(L)$ asymptotically approaches

316   the constant values z_{sn} as $|L| \to \infty$ and $z_s(L) = 4.5$ m as $|L| \to 0$. $z_s(L_{fc}) = z_{sfc} = 7.2$ m (see Table 1).

317

318   The dotted vertical lines correspond to $|L_{fc}| = 3.6$ m (left) as determined previously (see

319   Table 1), and the value of $|L_{tr}| = 120$ m (right) for which $z_s(L) = z_{tr}(L)$, i.e. for which

320   the logarithmic and convective contributions to $U(z)$ are equally important. For $|L| > 400$

321   m the logarithmic portion of $U(z)$ is overwhelmingly dominant compared to the

322 convective one, and therefore it can be considered that the ABL is in nearly neutral
323 conditions. For $L = L_{fc}$ or lower, the opposite is true, as the flow is nearly in free-
324 convection conditions. $z_s(L)$ physically behaves as expected, tending asymptotically to
325 constant values at each extreme of the stability interval (4.5 m as $|L| \rightarrow 0$, and z_{sn} for
326 $|L| \rightarrow \infty$). Figure 1 illustrates the way in which the surface layer becomes thinner with
327 increasing unstable stratification, because of the progressively higher buoyant production
328 of E in the mixed layer as $|L|$ decreases.

329

330 3.3 Behaviour of u_* as a function of L
331 Figure 2 presents u_* as a function of $|L|$, normalized by u_{*n}. The solid line corresponds
332 to $u_*(L)$ computed from (15), and the dash-dotted line extends the constant neutral value,
333 u_{*n} = 0.35 m s^{-1}, over the whole stability interval, for comparison. Figure 2 shows that
334 $u_*(L)$ decreases with decreasing $|L|$ until it reaches its minimum value (u_{*min}) at $L =$
335 $|L_{min}|$. According to (15), for $|L| < |L_{min}|$, $u_*(L)$ would increase monotonically with
336 decreasing $|L|$, in such a way that $u_*(L) \rightarrow \infty$ for $|L| \rightarrow 0$. This behaviour occurs
337 because, as $|L| \rightarrow 0$, the term between brackets on the right-hand side of (15) tends to
338 infinity. This is a consequence of the physically unrealistic behaviour of MOST as $|L| \rightarrow$
339 0, producing singularities. For this reason, in Fig. 2 we have assumed that $u_*(L) = u_{*min}$,
340 for $|L| \leq |L_{min}|$.
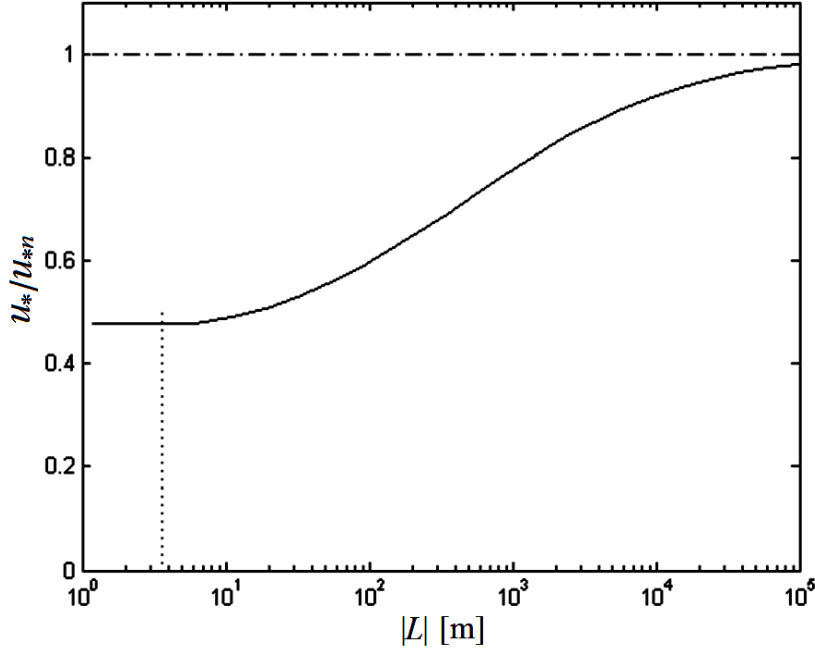
341

348 As can be seen in Fig. 2, $u_*(L)$ shows the expected physical behaviour (cf. Fig. 3.7 of

349 Garratt 1992), approaching asymptotically (by design) u_{*n} as $|L| \to \infty$, and decreasing

350 monotonically with decreasing $|L|$. However, the approach to u_{*n} as $|L| \to \infty$ is very

351 gradual and u_* only takes a value mid-way between the neutral and free-convection limits

352 for an $|L|$ of several hundred metres. Furthermore, the minimum value reached by $u_*(L)$

353 is u_{*min} = 0.17 m s^{-1} for L_{min}= 3.4 m. Thus, $u_{*min} = u_{*fc}$ and $|L_{min}|$ almost coincides

354 with $|L_{fc}|$= 3.6 m, determined previously (see Table 1). This result further confirms that

355 the assumption of constant $(\partial U/\partial z)_{z_s}$ is realistic, and allows obtaining reliable estimates

356 of u_* over the whole stability interval.

357 Although u_{*fc}, is thus a minimum value of u_*, it is generally not as low compared with

358 u_{*n} as might be expected. The case under consideration here, where $u_{*fc}/u_{*n} \approx 0.5$,

359 which is not particularly low (see Sect. 3.1, Table 1), is a good example. This result

360 ultimately suggests that a purely-thermal regime is unlikely (it was not realized in the

361 C94 measurements, in particular). For these reasons, under nearly free-convection

14

362 conditions both u_{*fc} and L_{fc} differ substantially from zero, as is confirmed by the

363 observations of K76 (see Table 2), and further corroborated for a very unstable surface-

364 layer case by Steeneveld et al. (2005). This is what allows MOST to be used here for

365 describing a highly convective ABL.

366

367 3.4 Flow speed-up calculation

368 Since calculating $\Delta S(L)$ using the HLR model requires knowing $u_*(L)$, the main purpose

369 of this section is to use the behaviour of $\Delta S(L)$ predicted by that model to indirectly

370 assess the dependence on stability of $u_*(L)$ (and also of $z_s(L)$) established in the method

371 proposed here, by comparison with values of ΔS measured over a wide range of L by

372 C94, and simulated numerically using the FLEX model.

373 Suppose that at a hilly location $\Delta S(L)$ needs to be estimated, assuming that the only

374 available parameters are z_0 and the mean wind speed, $U(z)$, measured at a suitably low

375 height such that, according to MOST, (11) is approximately valid for any L. Equation 11

376 can then be used for estimating u_{*n}. Once z_0 and u_{*n} are known, the present method

377 allows systematically obtaining $z_s(L)$, then $u_*(L)$ and finally $\Delta S(L)$, for the whole

378 unstable stratification parameter range.

379 In the specific case under consideration here, first using as input parameters $u_{*n} = 0.35$ m

380 s^{-1} and $z_0 = 0.05$ m (from C94), $u_*(L)$ is calculated using the proposed method. Next, this

381 $u_*(L)$ is used in the HLR model applied to flow over Cooper's ridge to calculate $\Delta S(L)$.

382 $\Delta S(L)$ is also calculated assuming that $u_* = const. = u_{*n}$, regardless of the observed L.

383 This simpler choice, often used for estimating $\Delta S(L)$ in flow over orography (e.g. W97),

384 is what the present approach aims to improve. Finally, the ΔS values are compared, for a

385 range of L, between the HLR model, the C94 measurements, and the FLEX model.

386 For the sake of simplicity the HLR and FLEX models are not described in detail here. A

387 brief description of the HLR model can be found in W97 or A09. FLEX is a microscale-

388 mesoscale, nonlinear and non-hydrostatic model, which was developed and validated

389 against experimental and field data by Argaín (2003) and A09. This model has been

390 tested and used extensively, namely by Teixeira et al. (2012, 2013a, 2013b) for assessing

391 analytical mountain wave drag predictions in 2D flows by comparison with numerical

392 simulations.

393   All the numerical simulations presented here used a main grid of (160×364) points for a

394   domain of (8000×2000) m size. The horizontal domain extent is $20a$ ($7a$ upstream of

395   the ridge maximum and $13a$ downstream). From $z = 40$ m downward the level of grid

396   refinement is gradually increased, and the lowest level is at a similar distance to the

397   surface as the observations (≈ 0.15 m). At the surface a no-slip condition is used, and

398    $\left(\overline{w'\theta}\right)_0$ and other turbulent quantities (turbulent kinetic energy, E, and dissipation ε of

399   E), are specified, for each L, by assuming that viscous dissipation balances shear and

400   buoyancy production. At the upper boundary, constant U and θ are prescribed, and L and

401   the derivatives of E and ε are set to zero.

402   Observations, and both theoretical and numerical predictions of ΔS as a function of $|L|$

403   are shown in Fig. 3, at $z = 8$ m and $z = 16$ m. The HLR model is applied in two cases: a)

404    $u_* = u_{*n}$, regardless of $|L|$ (dashed line), and b) the friction velocity is calculated for each

405    $|L|$, using the method proposed here (15) (solid line).

406

407
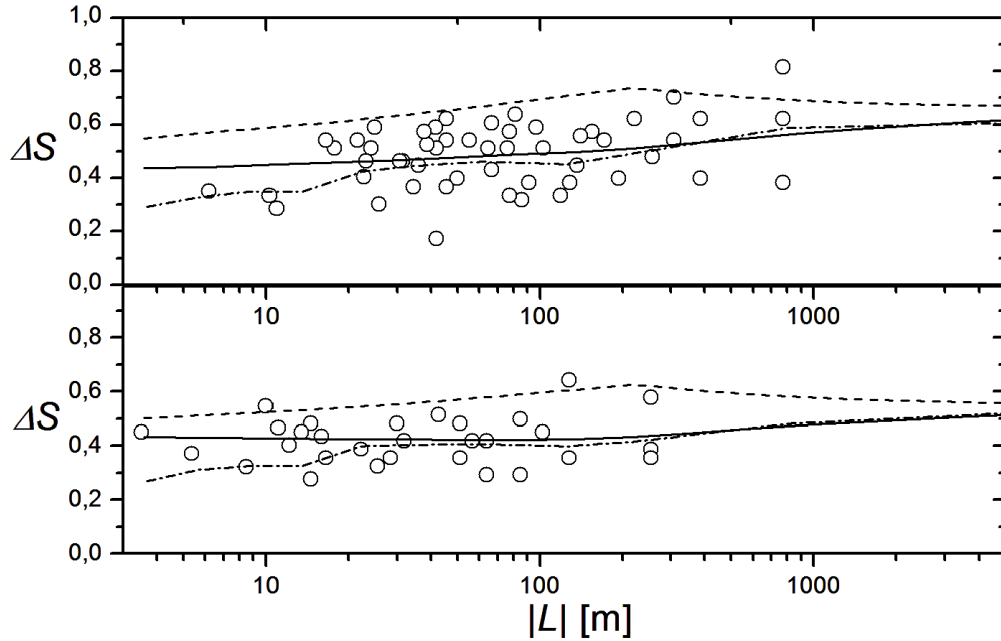
408   **Fig 3** Variation of the fractional speed-up (ΔS) as a function of stability, above the hill crest, at the heights

409    $z = 8$ m (top) and $z = 16$ m (bottom). Solid line: u_* computed using (15); dotted line: u_* kept constant,

410   regardless of the stability, and equal to the neutral ABL value ($u_{*n} = 0.35$ m s^{-1}); dash-dotted line: FLEX

411   model; symbols: observations from C94.

412

413   The significant differences between the ΔS curves, obtained using the two different

414   definitions of u_*, reveals that ΔS is very sensitive to the dependence of u_* on $|L|$, as

415   shown by A09 for the stable case. The results assuming $u_* = u_{*n}$ (dashed lines)

416   overestimate the observations considerably. In both panels of Fig. 3, the improvement in

417   the performance of the theoretical model, owing to the new method of calculating u_*

418   (solid lines), is significant over the whole stability interval. In general, this new method

419   produces results much closer to both the field measurements (despite the considerable

420   scatter in the data) and the numerical simulation results. ΔS calculated from the

421   theoretical model with u_* depending on L has a rather flat variation with $|L|$, especially at

422    $z = 16$ m, and although decreasing more substantially with $|L|$ at $z = 8$ m, slightly

423   overestimates both the measurements and the numerical simulations for the lowest values

424   of $|L|$.

425

426
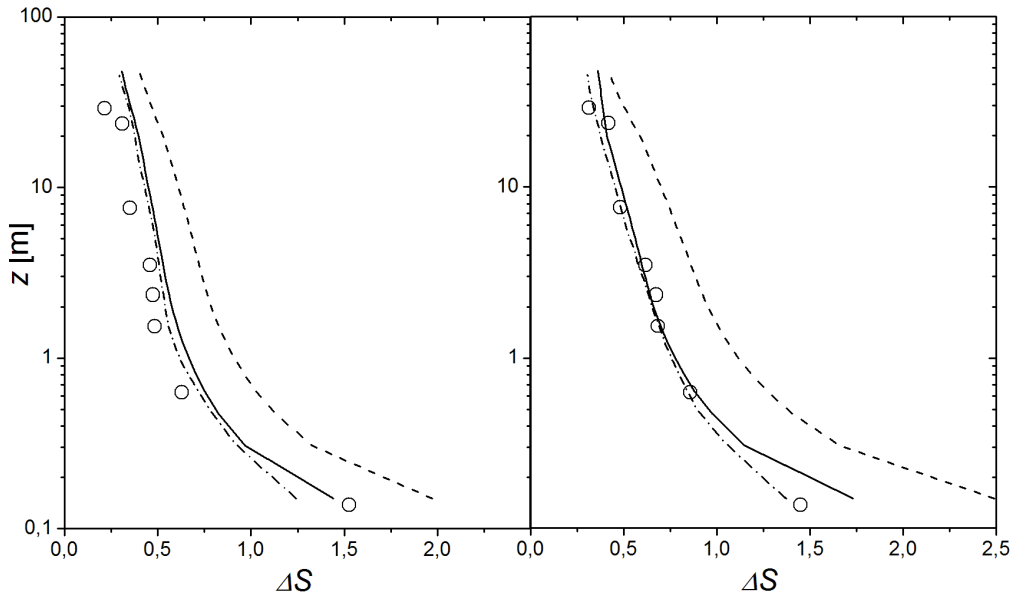
Fig 4 Profiles of the fractional speed-up ratio (ΔS) above the hill crest, for $|L| = 33$ m (left) and $|L| = 222$ m

(right). Solid line: u_* computed using (15); dashed line: u_* kept constant at $u_{*n} = 0.35$ m s^{-1}; dash-dotted

line: FLEX model; symbols: observations from C94.

430

431   Profiles of observations (C94), and both theoretical and numerical predictions of ΔS

432   directly above the hill crest, for $|L| = 33$ m (left panel) and $|L| = 222$ m (right panel) are

433   shown in Fig. 4. $|L| = 33$ m and $|L| = 222$ m correspond to strong and moderately weak

434   unstable stratification, respectively. In both cases, the proposed method compares better

435   both with the numerical model and with the field data, although it slightly overestimates

436   the observations in the more unstable case. Nevertheless, a general decrease of ΔS as one

437   shifts from the higher to the lower $|L|$ value is qualitatively reproduced. Given the

438   precision of the measurements and flow assumptions, not too much importance should be

439   attached to this overestimate, which also occurs in the numerical simulations

440   (consistently, a similar discrepancy can be detected for the theoretical model on the far

441   left of Fig. 3 at $z = 8$ m).

442   ΔS is much more severely overestimated, in both cases, by the profiles with a prescribed

443   constant $u_* = u_{*n}$, due essentially to the significant fractional deviation between u_{*n} and

444   the more accurate value of u_* determined from (15). This fractional deviation amounts to

445   ~45% for $|L| = 33$ m and to ~ 35% for $|L| = 222$ m (see Fig. 2), but this does not translate

446   into proportional deviations for ΔS, as the value of ΔS, where u_* is calculated from (15),

447   actually becomes closer to that where $u_* = u_{*n}$ as $|L|$ decreases (see Fig. 3). The fact that

448   there is such a large difference in the results using $u_*(L)$ and $u_* = u_{*n}$ for the weakly

449   unstable case might seem suspect, but Fig. 2 explains it, since for $|L| = 222$ m, $u_*(L)$ still

450   differs very substantially from u_{*n}.

451   It should be pointed out that at the lowest measurement level, ΔS should depend very

452   weakly on L, because near enough to the ground the flow is always approximately

453   neutral. The overestimate of the measured ΔS at that level by the theoretical model for $|L|$

454    $= 222$ m can probably be attributed to an inherent bias of the HLR solution, noted by

455   W97 and A09.

456

457   **4 Summary and conclusions**

458   In this paper, we propose a new method for estimating two scaling parameters of the

459   ABL: the surface-layer height z_s and the friction velocity u_*, as a function of stability

460   (quantified by the Obukhov length scale L), for an unstable ABL. These two parameters

461   are important for characterizing the unstable ABL, in particular its coupling with the

462   overlying convective mixed layer. Moreover, a correct estimation of u_*, whose

463   dependence on L is often not accounted for in a physically consistent way, is crucial for

464 producing accurate predictions of the speed-up (ΔS) in flow over hills, which is relevant
465 for a number of engineering applications.

466 Using a physical approach that is developed specifically for unstable conditions, via a
467 combination of MOST and convective mixed-layer scaling, our model takes into account
468 the fact that z_s decreases as the unstable stratification becomes stronger, due to erosion of
469 the surface-layer eddies by more energetic buoyancy-dominated eddies from the
470 convective mixed layer. The model also takes into account the fact that u_* decreases as
471 the ABL becomes more unstable, attaining a minimum value, but does not, in general,
472 approach zero in the free-convection limit, unless the wind vanishes completely (in which
473 case the concept of ΔS loses its meaning). The variation of u_* affects the turbulent fluxes
474 of various properties, and consequently the mean profiles of those properties, including
475 the wind speed $U(z)$, which determines the behaviour of ΔS.

476 Procedures to obtain boundary-layer parameters in the neutral and free-convection
477 regimes, and for bridging across these regimes, to cover the complete unstable ABL
478 parameter range, were developed and tested using available field data. The performance
479 of the model was then evaluated more comprehensively, by comparing predictions of ΔS
480 in unstable conditions, using the linear model of HLR incorporating the new friction
481 velocity formulation, against measurements from C94, and numerical simulations of the
482 FLEX mesoscale-microscale model. Agreement was found to be substantially improved
483 relative to results where u_* is held constant. This emphasizes the importance of
484 accounting for the full dynamics of the unstable ABL, including the variation of u_* and z_s
485 with stability, for correctly estimating ΔS. The proposed method, whose possible
486 applications are not limited to improving the calculation of ΔS, should be seen as a
487 preliminary step in the development of better tools for the parametrization of unstable
488 ABLs. Further validation of this method by comparison with observations remains
489 necessary.

490

496

Appendix 1. Accuracy of the $(\partial\theta/\partial z)_{z_s} = const.$ approximation

In the present model, the form of $z_s(L)$ is established using the temperature gradient $\partial\theta/\partial z$, which can be obtained from (2) and (4), yielding

$$\frac{\partial\theta}{\partial z} = \theta_*'\left[1 + \gamma_h\left(\frac{z}{|L|}\right)^{\alpha_1}\right]^{-\alpha_2} z^{-1}, \qquad (18)$$

where $\theta_*' = Pr_t\theta_*/\kappa$. According to (18), $\partial\theta/\partial z \to 0$ as $z \to \infty$. This is consistent with the assumption that $\theta = const.$ in the mixed layer, so, at $z = z_s$ the derivative $(\partial\theta/\partial z)_{z_s}$ should be suitably small, and this smallness is exploited to obtain z_s. Note that a similar condition could be based on the mean velocity gradient (1), but we think that $\theta = const.$ is more reliable in the mixed layer, since $U(z)$ profiles may exhibit non-negligible shear above the surface layer, due to variation of the pressure perturbation induced by the orography with height or the Coriolis force. Taking this into account, the ratio

$$\Psi(z_s, L) = \frac{(\partial\theta/\partial z)_{z_s}}{(\partial\theta/\partial z)_{z_{0\theta}}} = \left[\frac{1 + \gamma_h(z_s/|L|)^{\alpha_1}}{1 + \gamma_h(z_{0\theta}/|L|)^{\alpha_1}}\right]^{-\alpha_2} \frac{z_{0\theta}}{z_s}, \qquad (19)$$

implicitly determines $z_s(L)$, if the form of the function $\Psi(z_s, L)$ is known. In (19) $(\partial\theta/\partial z)_{z_s}$ and $(\partial\theta/\partial z)_{z_{0\theta}}$ are obtained by evaluating (18) at z_s and the temperature roughness height, $z_{0\theta}$, respectively. As defined by (19), $\Psi(z_s, L)$ varies monotonically from 1 to zero as $z_{0\theta}/z_s$ decreases. Moreover, $\Psi(z_s, L)$ depends only weakly on L: by substituting L_{fc}, z_{sfc}, z_{sn} and $L_n = \infty$ (see Sect. 3.1, Table 1) into (19) we may calculate the ratio $\Gamma = \Psi(z_{sn}, L \to -\infty)/\Psi(z_{sfc}, L_{fc}) \approx 0.6$, which is of order 1.

The limits of $\Psi(z_s, L)$ at the theoretical extremes of the stability interval are, respectively,

$$\Psi_{sfc} = \Psi(z_{sfc}, L \to 0) = \lim_{|L| \to 0} \Psi(L) = \left(\frac{z_{0\theta}}{z_{sfc}}\right)^{\alpha_1\alpha_2+1}, \qquad (20)$$

$$\Psi_{sn} = \Psi(z_{sn}, L \to \infty) = \lim_{|L| \to \infty} \Psi(L) = \frac{z_{0\theta}}{z_{sn}}. \qquad (21)$$

For both strongly and weakly unstable flows, (20) - (21) suggest that $\psi(z_s, L) \propto (z_{0\theta}/z_s)^{\alpha}$, where α is a dimensionless constant. Taking this result into account, we

hypothesize that this form holds for the whole stability interval, yielding the following

approximate definition for $\psi(z_s, L)$,

$$\Psi(z_s, L) = \alpha_{\Psi 2} \left(\frac{z_{0\theta}}{z_s} \right)^{\alpha_{\Psi 1}} , \qquad (22)$$

where $\alpha_{\Psi 1}$ and $\alpha_{\Psi 2}$ are dimensionless constants. These two constants can be determined

by taking the limits of (22) in the free-convection and neutral regimes, and comparing the

corresponding expressions with (20) and (21), respectively. This produces a set of two

equations, which may be solved for $\alpha_{\Psi 1}$ and $\alpha_{\Psi 2}$, yielding

$$\alpha_{\Psi 1} = \ln \left[\frac{\Psi(z_{sn}, L \to \infty)}{\Psi(z_{sfc}, L_{fc})} \right] \Bigg/ \ln \left(\frac{z_{sfc}}{z_{sn}} \right) \qquad \alpha_{\Psi 2} = \Psi(z_{sfc}, L_{fc}) \left(\frac{z_{0\theta}}{z_{sfc}} \right)^{-\alpha_{\Psi 1}} \qquad (23)$$

By combining (19) and (22), (14) is obtained.

Appendix 2. Accuracy of the $(\partial U / \partial z)_{z_s} = const.$ approximation

Here we show that the approximation $(\partial U / \partial z)_{z_s} = const.$, used in Sect. 2.4 for

evaluating u_*, is supported by measurements. Let us consider the following ratio, by

using MOST,

$$\beta_{MOST} = \frac{(\partial U / \partial z)_{z_{sn}}}{(\partial U / \partial z)_{z_{sfc}}} = \underbrace{\left(\frac{c_{fc} \beta_1 |f|}{c_{SL} c_{zin}} \right)}_{\alpha_5} \frac{|L_{fc}|}{u_{*fc}} , \qquad (24)$$

where $\beta_1 = \left(1 + \gamma_m c_{fc}^{\alpha_1} \right)^{\alpha_2}$. Equation 24 is obtained by combining (1), (4), (6), (12) and

(13). Using parameters from C94 (see Sect. 3.1) we obtain $\alpha_5 = 0.0466$ s^{-1}. For the values

of L_{fc} and u_{*fc} shown in Table 1, this yields $\beta_{MOST} = 0.99$. The remarkable closeness of

this value to 1 is fortuitous, although it obviously depends on the values adopted for c_{zin},

c_{fc} and c_{SL}. For checking further the approximation $\beta_{MOST} \approx 1$ we use the K76

observations (keeping the same α_5), which were carried out in a daytime well-mixed

CBL, with evidence of significant heat and momentum entrainment through the capping

inversion.

Run	u_{*fc} (m s^{-1})	$|L_{fc}|$ (m)	z_{ifc} (m)	w_* (m s^{-1})	w_*/z_{ifc} (s^{-1})	β_{MOST}
6A1	0.24	5.7	2095	2.43	1.16×10^{-3}	1.1

| 6A2 | 0.23 | 6.4 | 2035 | 2.21 | 1.09×10^{-3} | 1.3 |

Table 2 CBL parameters measured by Kaimal et al. (1976). Columns 6 and 7 show, respectively, w_*/z_{ifc}, and β_{MOST}, calculated from the data (the second quantity by using (24)).

Table 2 shows CBL parameters obtained by K76, corresponding to the runs with the smallest values of $|L|$, typical of nearly free-convection regimes. As can be seen, the values of β_{MOST} are close to 1, corroborating the hypothesis $\beta_{MOST} \approx 1$. Moreover, column 6 supports (10), proposed by Venkatram (1978), since $c_5 = w_*/z_{ifc}$ varies within a narrow range. Venkatram (1978) estimated $c_5 = 1.12 \times 10^{-3}$ s^{-1}, which is quite close to both values shown in Table 2. Therefore, the assumption that c_5 is a constant is plausible. If the assumption $\beta_{MOST} = 1$ is accepted, (24) defines a relationship between α_5, $|L_{fc}|$ and u_{*fc}. If parameters c_{fc} and c_{zin} are assumed to be non-adjustable, this is equivalent to a relation between $|L_{fc}|$, u_{*fc} and c_{SL}. Equation 13 is only applicable if $|L| \rightarrow \infty$ (a rarely observed situation), so the parameter c_{zin} may have a considerable uncertainty. Zilitinkevich et al. (2012) and Garratt (1992) discuss this topic at length. It would be interesting to explore the constraint defined by (24) further to develop relations other than (13) for estimating z_{in}, but that is beyond the scope of the present paper.

We also carried out a similar analysis using the classical free-convection formulation of Prandtl (1932) for the mean velocity gradient,

$$\left(\frac{\partial U}{\partial z}\right)_{z_{sfc}} = \frac{c_u u_{*fc}(\kappa \, |L_{fc}|)^{1/3}}{z_{sfc}^{4/3}} = \frac{c_u \kappa^{1/3}}{c_{fc}^{4/3}} \frac{u_{*fc}}{|L_{fc}|}, \qquad (25)$$

where $c_u = 1.7$. In this case we would obtain a ratio $(\partial U/\partial z)_{z_{sfc}}/(\partial U/\partial z)_{z_{sn}}$ with a similar parameter dependence as (24) and $\alpha_5 = 0.0453$ s^{-1}. The proximity between the values of α_5 obtained using both formulations for $(\partial U/\partial z)_{z_{sfc}}$ confirms that the MOST formulation adopted here is physically consistent, hence it may be used to describe the free-convection regime.

References

Argaín JL (2003) Modelação de Escoamentos Atmosféricos: Efeitos Orográficos e de Camada Limite (in Portuguese). Ph.D. Thesis, Universidade do Algarve, 275 pp

572   Argaín JL, Miranda PMA, Teixeira MAC (2009) Estimation of the friction velocity in stably stratified
573   boundary-layer flows over hills. Boundary-Layer Meteorol 130: 15-28

574   Businger JA (1973) A Note on Free Convection. Boundary-Layer Meteorol 4: 323–326

575   Coppin PA, Bradley EF, Finnigan JJ (1994) Measurements of flow over an elongated ridge and its thermal
576   stability dependence: The mean field. Boundary-Layer Meteorol 69: 173-199

577   Deardorff JW (1970) Convective velocity and temperature-scales for the unstable planetary boundary layer.
578   J Atmos Sci 27: 1211–1213

579   Garratt JR (1992) The Atmospheric Boundary Layer, Cambridge University Press, 316 pp

580   Hunt JCR, Leibovich SL, Richards KJ (1988) Turbulent Shear Flows Over Low Hills. Q J R Meteorol Soc
581   29: 16-26

582   Kader BA, Yaglom AM (1990), Mean Fields and Fluctuation Moments in Unstably Stratified Turbulent
583   Boundary Layers, J Fluid Mech 212: 637–662

584   Kaimal JC, Wyngaard JC, Haugen DA, Cote OR, Izumi Y, Caughey SJ, Readings CJ (1976) Turbulence
585   Structure in the Convective Boundary Layer. J Atmos Sci 33: 2152-2169

586   McNaughton KG (2004) Turbulence Structure of the Unstable Atmospheric Surface Layer and Transition
587   to the Outer Layer. Boundary-Layer Meteorol 112: 199-221

588   Prandtl L (1932) Meteorologische Anvendungen der Strömungslehre. Beitr Phys Fr Atmos 19: 188-202

589   Rossby CG, Montgomery RB (1935) The layers of frictional influence in wind and ocean currents. Pap
590   Phys Oceanogr Meteorol 3: 101 pp

591   Schumann U (1988) Minimum Friction Velocity and Heat Transfer in the Rough Surface Layer of a
592   Convective Boundary Layer. Boundary-Layer Meteorol 44: 311–326

593   Steeneveld GJ, Holtslag AAM, DeBruin HAR (2005) Fluxes and gradients in the convective surface layer
594   and the possible role of boundary-layer depth and entrainment flux, Boundary-Layer Meteorol 116:
595   237-252

596   Stull, RB (1988) An Introduction to Boundary-Layer Meteorology, Kluwer Academic Publishers,
597   Dordrecht,, 670 pp

598   Stull, RB (2011) Meteorology for Scientists and Engineers, 3rd edition, University of British Columbia,
599   Vancouver British Columbia, 938 pp

600   Sykes RI, Henn DS, Lewellen WS (1993) Surface-layer description under free-convection conditions. Q J
601   R Meteorol Soc 119: 409–421

602   Teixeira MAC, Argaín JL, Miranda PMA (2012) The importance of friction in mountain wave drag
603   amplification by Scorer parameter resonance. Q J R Meteorol Soc 138: 1325-1337

604   Teixeira MAC, Argaín JL, Miranda PMA (2013a) Drag produced by trapped lee waves and propagating
605   mountain waves in a two-layer atmosphere. Q J R Meteorol Soc 139: 964-981

606   Teixeira MAC, Argaín JL, Miranda PMA (2013b) Orographic drag associated with lee waves trapped at an
607   inversion. J Atmos Sci 70: 2930–2947

608   Venkatram A (1978) Estimating the convective velocity scale for diffusion applications. Boundary-Layer
609   Meteorol 15: 447-452

610   Von Engeln A and Teixeira J (2013) A planetary boundary-layer height climatology derived from ECMWF
611   re-analysis data. J. Clim 26: 6575–6590

612   Weng W (1997) Stably stratified boundary-layer flow over low hills: A comparison of model results and
613   field data. Boundary-Layer Meteorol 85: 223-241

614   Weng W, Taylor PA (2003) On modelling the one-dimensional atmospheric boundary layer. Boundary-
615   Layer Meteorol., 107:371-400

616   Wilson DK (2001) An Alternative Function for the Wind and Temperature Gradients in Unstable Surface
617   Layers. Boundary-Layer Meteorol 99: 151–158

618   Zilitinkevich SS (1995) Non-local turbulent transport: Pollution dispersion aspects of coherent structure of
619   convective flows. Air Pollution Theory and Simulation. Power H, Moussiopoulos N, Brebbia CA, Eds.,
620   Vol. I, Air Pollution III, Computational Mechanics Publications, 53–60.

621   Zilitinkevich SS, Hunt JCR, Grachev AA, Esau IN, Lalas DP, Akylas E, Tombrou M, Fairall CW,
622   Fernando HJS, Baklanov AA, Joffre SM (2006) The influence of large convective eddies on the
623   surface-layer turbulence. Q J R Meteorol Soc 132: 1423-1456

624   Zilitinkevich SS, Tyuryakov SA, Troitskaya YI, Mareev EA (2012) Theoretical Models of the Height of
625   the Atmospheric Boundary Layer and Turbulent Entrainment at Its Upper Boundary. Izvestiya,
626   Atmospheric and Oceanic Physics 48(1): 133-142